Hindawi Publishing Corporation
International Journal of Photoenergy
Volume 2015, Article ID 170507, 9 pages
http://dx.doi.org/10.1155/2015/170507

Research Article

Improving Efficiency of Evaporated Cu_2ZnSnS_4 Thin Film Solar Cells by a Thin Ag Intermediate Layer between Absorber and Back Contact

Hongtao Cui, Chang-Yeh Lee, Wei Li, Xiaolei Liu, Xiaoming Wen, and Xiaojing Hao

School of Photovoltaic and Renewable Energy Engineering, University of New South Wales, Sydney, NSW 2052, Australia

Correspondence should be addressed to Hongtao Cui; h.cui@unsw.edu.au and Xiaojing Hao; xj.hao@unsw.edu.au

Received 12 November 2014; Revised 29 December 2014; Accepted 30 December 2014

Academic Editor: Raghu N. Bhattacharya

A 20 nm Ag coating on Mo back contact was adopted to improve the back contact of evaporated Cu_2ZnSnS_4 (CZTS) solar cells. The Ag layer helped reduce the thickness of MoS_2 which improves fill factor (FF) significantly; additionally, it reduced secondary phases ZnS and SnS_{2-x}, which may help carrier transport; it was also involved in the doping of the absorber layer, which compensated the intrinsic p-type doping and therefore drags down the doping level. The doping involvement may enlarge the depletion region and improve lifetime of the absorber, which led to enhancing open circuit voltage (V_{OC}), short circuit current density (J_{SC}), and efficiency significantly. However, it degrades the crystallinity of the material slightly.

1. Introduction

Cu_2ZnSnS_4 (CZTS) is one of the most promising thin film solar cell absorber candidates owing to its earth abundance, direct band gap with the optimal value ~1.45 eV, and environment compatible nature [1]. The development of this technology is based on mature commercialized $CuIn_XGa_{1-X}Se_2$ (CIGS) technology which shares similar crystal structure, electronic band structure, and high absorption coefficient [1]. The champion efficiency of CZTSSe solar cells is only 12.6% in contrast with that of CIGS counterpart 21.7% [2], indicating a big potential and challenge for the former. Mo as the back contact needs reexamination due to the reaction between Mo and CZTS which leads to the formation of defects especially voids and secondary phases in the vicinity of back contact region which are detrimental to device performance [3–6]; the voids are left by evaporation of SnS and a Kirkendall type interdiffusion with high Cu, Zn, and Sn updiffusion to the surface and low S diffusion into the metal, which may form shunting path [7]; secondary phases such as ZnS, SnS_2 may form carrier transport barrier [7]. Also, a high sulphur (S) pressure is needed to suppress the decomposition of CZTS on the top surface and also reaction between CZTS and Mo in the back contact region. Moreover, high S pressure avoids the deep level S vacancy defect [8]. However, it causes the formation of a highly resistive thick MoS_2 layer [3, 4, 6]. On the other hand, adequate thin MoS_2 or $MoSe_2$ is benign to the device owing to the good adhesion and quasi-ohmic contact with the absorber [9, 10]. To inhibit the formation of a thick $MoSe_2$ layer, as well as the voids and the secondary phases at the back contact, barrier layers such as TiN [11], ZnO [12, 13], and TiB [14] have been proved effective and therefore enhance the device performance dramatically. Additionally, a 20 nm Ag coating on Mo was also found effectively reducing voids, secondary phases, and MoS_2 and involved in the formation of $(Ag,Cu)_2ZnSnS_4$; the Ag layer degraded the crystallinity slightly though. Consequently, it improved V_{OC}, J_{SC}, FF, series resistance, and efficiency substantially for sputtered CZTS solar cells [15]. However, the distribution of Ag inside the film and its influence on the doping of the absorber are not yet clear, which will be investigated in this paper.

Besides this, evaporation is one of the main stream deposition methods for CIGS solar cells and the focus of this paper is on evaporated CZTS precursor.

2. Materials and Methods

The reference SLG substrate had ~1000 nm thick Mo coated on it with a sheet resistance of ~0.15 Ω/□. The 20 nm Ag was

deposited on $5 \times 5\,cm^2$ Mo-coated soda lime glass substrate by thermal evaporation. Both substrates were subjected to CZTS precursor depositions. The precursors were deposited on the substrates by coevaporation of the metal elements at constant deposition rates in a Mantis thermal evaporator equipped with Cu, Zn, and Sn effusion cells (Veeco manufactured): Cu at ~0.7 Å/s, Zn at ~1.4 Å/s, and Sn at ~2.7 Å/s. During deposition, the substrates are rotated at 20 rev/min without intentional heating. The base pressure of the chamber is $\sim 3 * 10^{-8}$ Torr. Both precursors are then sulfurised at a dual zone tube furnace at 575°C in a sulphur (S) atmosphere for 5 min in a dual zone tube furnace (OTF-1200 MTI) with the S zone temperature retained at 300°C and N_2 flow rate at 20 sccm. The selection of 575°C was based on a previous investigation that the temperature resulted in less secondary phases and higher efficiency than lower temperature [16]. The rest of the device structure is completed via a standard process of chemical bath deposition of CdS, sputtering deposition of intrinsic ZnO (i-ZO), and Al doped ZnO (AZO). CdS deposition was conducted at ~80°C for ~80 nm with details described in [17]. The detail of i-ZO and AZO deposition was described elsewhere [15]. The i-ZO is adopted prior to AZO deposition to avoid damage to the absorber during AZO deposition and reduce AZO shunting through pinholes [18]. A conductive Ag glue is then pasted on the window layer as the top electrode and the cell area is defined by mechanical scribing to be $\sim 0.2\,cm^2$.

The chemical composition of the CZTS absorber films is estimated by a solution-based inductively coupled plasma (PerkinElmer Quadrupole NexION ICPMS). Renishaw inVia spectrometer coupled with a microscope is used to conduct Raman measurement with a 514 nm laser excitation. PANalytical's X'Pert pro materials research diffraction system is used to perform XRD measurement. The SEM images were taken in a FEI Nova NanoSEM230 system. xT Nova NanoLab 200 was used milling a 100–200 nm thick ~22 μm long cross section from a sample for transmission electron microscopy (TEM) measurement as in [16]. A FEI Tecnai G2 20 TEM operated at 200 kV and equipped with an energy dispersive spectroscopy (EDS) detected was used for microstructure and chemical elements distribution analysis. The QEX10 system (PV MEASUREMENTS Inc.) is utilised for external quantum efficiency (EQE) measurement. Light I-V measurement is performed at 25°C with the J_{SC} calibrated by EQE measurement. The capacitance-voltage (C-V) measurement was conducted by an impedance analyser (Hewlett Packard 4194A) to determine the doping density. Time-resolved photoluminescence (TRPL) was taken on the samples by the time correlated single photon counting (TCSPC) technique on a Microtime-200 system (Picoquant). A 470 nm laser was used as the excitation source with a repetition rate of 10 MHz. The PL evolution was detected by fast response avalanche photodiode through band-pass filter. The time resolution is determined as 200 ps by response function.

3. Results and Discussions

The chemical composition of the sulfurised CZTS film measured by ICP is Cu/(Zn + Sn)~0.88 and Zn/Sn~1.09. The Cu/(Zn + Sn) is whereas Zn/Sn is not in the desired range (Cu/(Zn + Sn) = 0.8-0.9, Zn/Sn = 1.2-1.3) reported for high efficiency CZTS solar cells [9].

Figure 1(a) is the XRD spectra of the absorbers with and without the Ag intermediate layer. It indicates that XRD of both films agrees with that of tetragonal kesterite CZTS (JCPDS number 026-0575) and that the Ag layer results in a clear left shift of the (112) peak by 0.17°. This suggests that Ag was involved in forming $(Cu,Ag)_2ZnSnS_4$. The distribution of Ag in sputtered CZTS sample was found to be uniform supporting the doping claim [19], which will be discussed in the evaporated sample case in the later part of this paper. The shift could be explained as follows. Ag has a larger atom size than Cu and lattice spacing will increase when Ag replaces Cu site. And, from Bragg's law, $n\lambda = 2d \sin\theta$, d increase leads to θ decrease (namely, left shift). Actually, (112) peak of Ag_2ZnSnS_4 (AZTS) and CZTS is 27.27° and 28.53°, respectively, AZTS left shifts the peak by as large as 1.56° [20]. Because Ag only acts as doping, only 0.17° left shift was seen. This doping also appears to broaden FWHM of the (112) peak from 0.182° to 0.19° and degrades the crystallinity of the absorber slightly, which might affect the V_{OC} of the device. The degraded crystallinity may be accounted for by lattice disorder introduced during Ag doping when replacing part of Cu site with Ag as Ag has a larger atom size than Cu. All the above agrees with findings in [15]. Nevertheless, both XRD patterns show Sn peaks, which may induce shunting especially for porous structure. The presence of Sn peak is due to a relatively low thermodynamic driving force (Gibbs free energy change of relevant reactions for forming each of the sulfides detailed in [13]) for formation of SnS or SnS_2 in comparison with ZnS, Cu_2S, and MoS_2 which leads to unreacted Sn isolated by reaction product stopping sulfurisation of inside Sn in condition of excess Sn, agreeing with our previous findings [13, 21]. Since XRD cannot distinguish CZTS, Cu_2SnS_3, and ZnS, Raman measurement is performed and the results are displayed in Figure 1(b). It shows dominant CZTS peaks at 337 cm^{-1} and 287 cm^{-1} with a blue shift for the sample with Ag layer. Raman measurement also reveals small wide SnS_{2-x} peaks in both films with slightly higher intensity for the sample without Ag layer and implies that SnS_{2-x} may be present in form of very small nanocrystallites and of trace amount because it was detected in Figure 1(a). Meanwhile, a small wide ZnS peak at ~353 cm^{-1} is present only in the sample without Ag because Ag acts like Cu and Ag containing sample has more elements (Cu and Ag) to react with ZnS and SnS_{2-x} with little unreacted left. Figure 1(b) also suggests that ZnS, SnS_{2-x} exist on the top subsurface region as the penetration depth of 514 nm Raman laser for CZTS absorber is ~100 nm which is generally in the space charge region [22] and may act as electron transport barriers. Figure 1(c) shows Raman spectra of both samples with the absorber mechanically removed as in [15]. The sample with Ag layer has much reduced MoS_2 peak consistent with findings in [15], which may suggest a reduced MoS_2 formation.

Figures 2(a) and 2(c) show high-angle angular dark-field (HAADF) images of absorbers without and with the Ag layer, respectively, which also marks the directions of EDS line

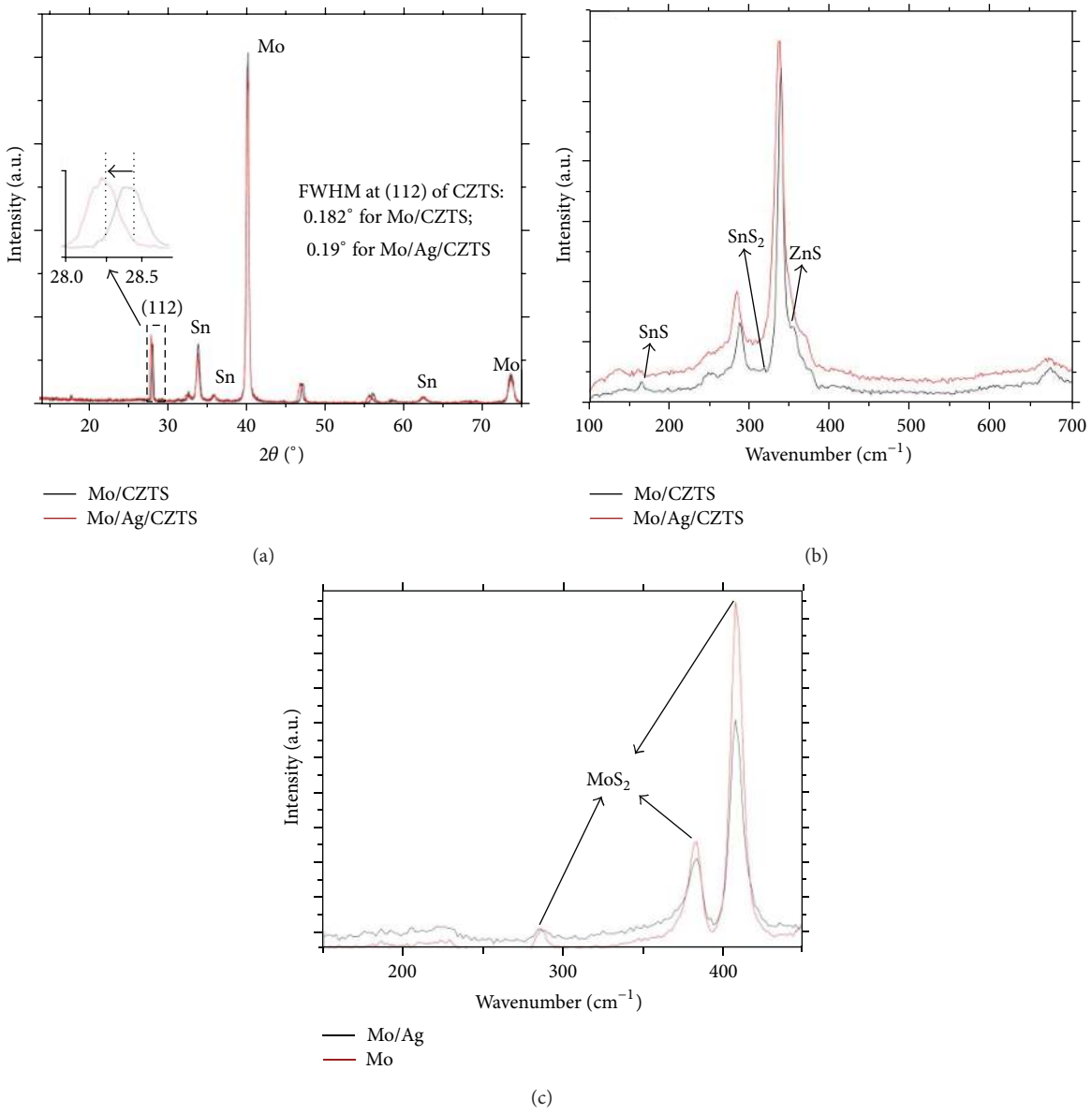

Figure 1: (a) X-ray diffraction (XRD) spectra of the CZTS thin films on Mo back contacts with and without the Ag intermediate layer; (b) Raman spectra of CZTS absorbers with and without 20 nm Ag intermediate layer; and (c) Raman spectra of samples in (a) with the absorber mechanically removed by the same method applied in [15].

scans; both reveal large connected voids at the back contact region. Figures 2(b) and 2(d) present the elemental profiles determined from the EDS line scans. Mo-K peak was used to characterise the Mo distribution. And since S-K and Mo-L peak overlaps, S signal actually reflects the combination of S and Mo. A Mo shoulder step is observed because of the formation of MoS_2 which gives rise to the weak Mo signal at the MoS_2 layer in comparison with Mo layer. The thickness of MoS_2 is ~150 nm for the sample with Ag layer and ~200 nm for the sample without Ag layer. Ag reacts with S or CZTS before Mo because it is coated on Mo. After the overcoating Ag layer is consumed, S or CZTS starts to react with Mo and form MoS_2. Consequently S or CZTS has less time to react with Mo. Therefore, the thickness of MoS_2 is reduced for sample with the Ag layer. Since MoS_2 is highly resistant and increases series resistance [11], the device with Ag layer may enjoy higher FF than device without Ag. Besides this, Sn hump is observed in both samples, which agrees with the findings in Figure 1(a).

To check the effect of the Ag layer on device performance, light I-V measurement is taken on 10 cells each for samples with and without the Ag intermediate layer, respectively. The measured V_{OC}, J_{SC}, FF, and efficiency are displayed in Figure 3. It indicates that the Ag layer improves all the IV parameters substantially. The uniformity issue even on the same sample is mainly introduced by precursor, window layer deposition, and sulfurisation process. The Zn, Sn crucible for thermal evaporation in our lab is only 20 cubic centimeters

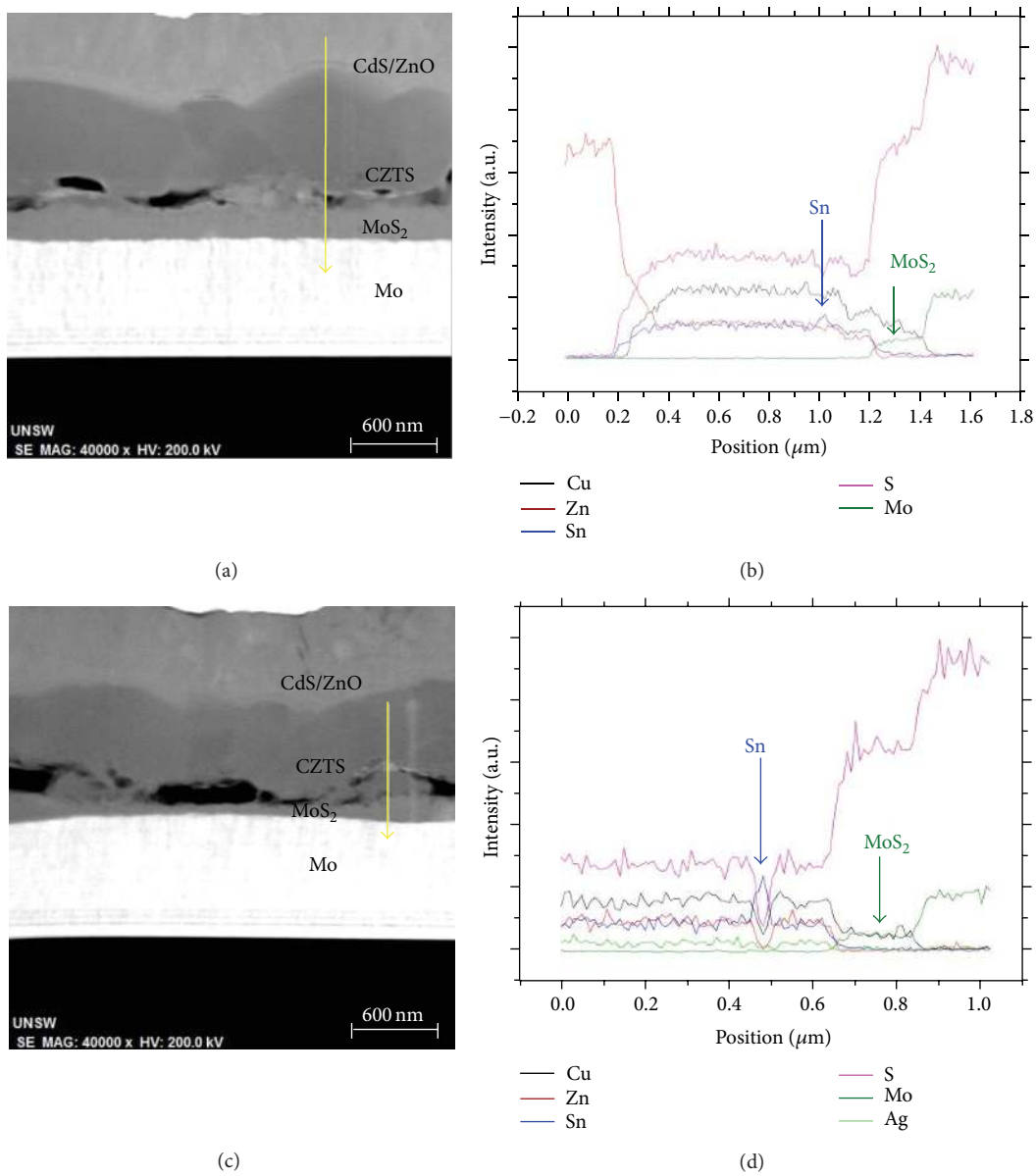

Figure 2: HAADF image of CZTS solar cells without (a) and with (c) Ag intermediate layer. The yellow arrow denotes the direction of an EDS line scan; (b) and (d) elemental profiles measured by the EDS line scans which are defined by the yellow arrow in (a) and (c), respectively.

large and allows within 3% film thickness uniformity as suggested by manufacturer. Similarly CdS, i-ZO, and AZO deposition may also have tiny uniformity issue. Even for sulfurisation process, it may introduce slight difference on the S flow facing side and the opposite side because the S flow facing side would have more annealing plateau time than the opposite side. All add up to the uniformity issue. The uniformity issue may lead to slight film thickness, composition, and roughness difference on the same sample, which may cause nonuniformity of V_{OC}, J_{SC}, FF, and efficiency. This phenomenon is common in laboratory fabrication of CZTS solar cells in a lab and would not be a problem for large scale production. To make a comparison on an individual cell level, the best cells of the samples with and without Ag are selected. *C-V*, TRPL, light *I-V*, external quantum efficiency (EQE), and reflection (R) measurements of both cells are taken and the results are illustrated in Figures 4–6. Internal quantum efficiency (IQE) is given by IQE = EQE/(1 − R) and is also shown in Figure 6.

The doping density can be estimated from the slope of $1/C^2$ versus V plot by the following relation [23]:

$$N_a = \frac{2}{q\varepsilon_0\varepsilon_s A^2 \left[(d/dV)\left(1/C^2\right)\right]}, \quad (1)$$

where N_a is the acceptor concentration, C is capacitance, V is voltage, q is the electron charge, ε_0 is permittivity of free space, ε_s is 10 (the dielectric constant) [24], and A is the area of the cell. The calculated results are 5.16×10^{19} cm^{-3} and 2.74×10^{17} cm^{-3}, respectively, as shown in Figure 4. For the sample

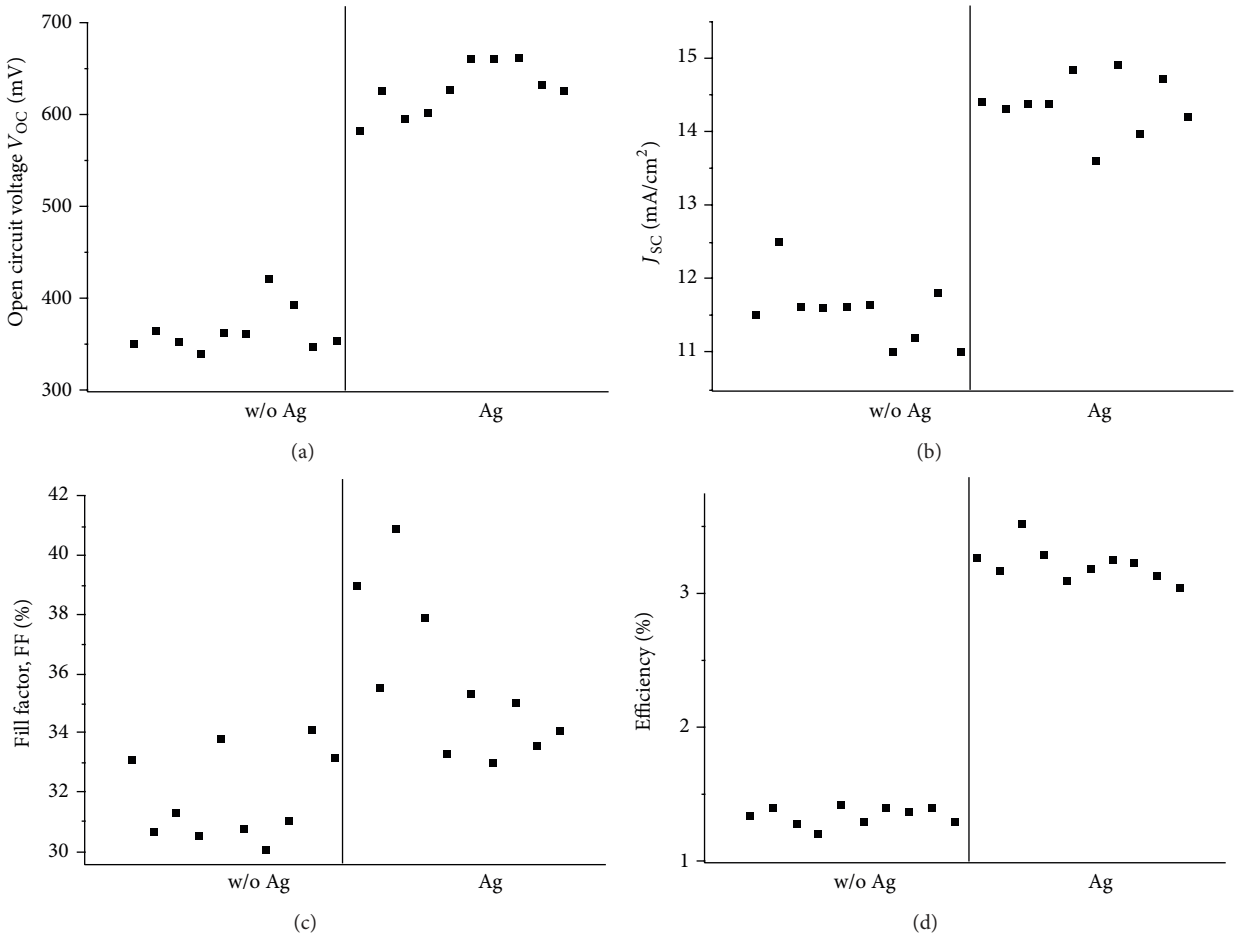

Figure 3: IV parameters of 10 CZTS solar cells each from the sample with and without the Ag intermediate layer: (a) open circuit voltage (V_{OC}); (b) short circuit current density (J_{SC}); (c) fill factor (FF); and (d) efficiency.

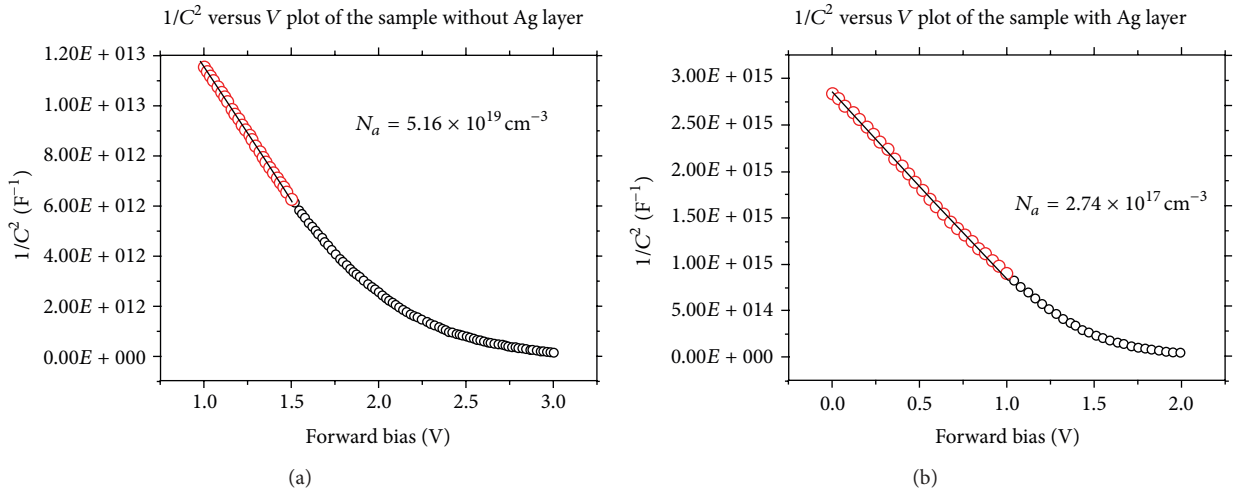

Figure 4: $1/C^2$ versus V plot of (a) the cell without Ag layer and (b) the cell with Ag layer. The slope is extracted by linear fitting of the linear data (red circles).

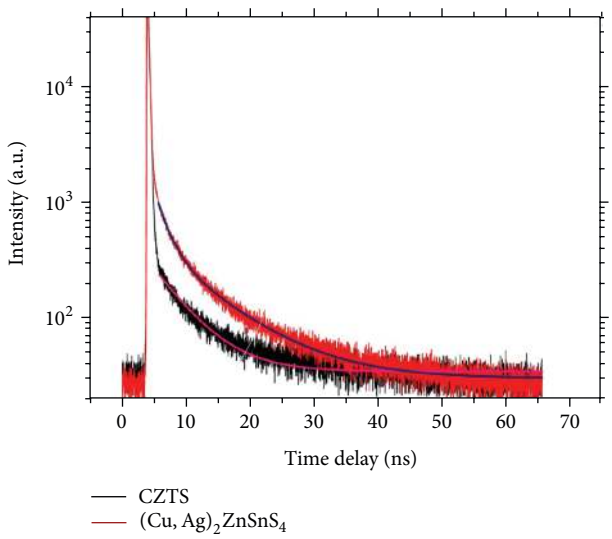

Figure 5: Time-resolved photoluminescence traces of absorbers fabricated with or without an Ag intermediate layer. The minority carrier lifetime can be obtained from curve fitting the data using equation (4). The blue and pink curves correspond to fitted ones for $(Cu,Ag)_2ZnSnS_4$ and CZTS, respectively.

without Ag layer, the doping concentration is higher than most of the values in previous studies [23–27], from the order 10^{16} to 10^{18} cm^{-3}. The reason for unusually high doping level can be caused by the detected SnS Raman peak in the CZTS film, since Sn vacancy defects in SnS form p-type doping [28, 29]. More importantly, the high Cu/(Zn + Sn) ratio leads to high Cu_{Zn} antisite, therefore a high p-type doping [30]. The significant decrease of doping concentration by adding an Ag layer is because of two main causes. (1) The Ag layer reduces the amount of acceptor concentration contributed by secondary phases, such as SnS, so the total acceptor density drops. (2) In the Ag doped CZTS film, Ag replaces Cu to form another quaternary compound, Ag_2ZnSnS_4 (AZTS), which plays a role as a donor doping in the CZTS film and therefore neutralises part of the p-type doping level [31, 32]. A similar study on $(Cu_xAg_{1-x})_2ZnSnS_4$ also showed Ag doping can convert CZTS to an n-type property [33]. The depletion region width can be estimated by the following equation using built-in voltage and doping concentration obtained through C-V measurement above [34]:

$$W_d = \sqrt{\frac{2\varepsilon_0\varepsilon_s V_{bi}}{qN_a}}, \tag{2}$$

where V_{bi} is the built-in voltage. The calculated depletion region width is 7 nm and 75 nm for the sample without and with Ag doping, respectively. The carrier collection depth is the sum of depletion region width and minority carrier diffusion length which is proportional to minority carrier lifetime. Minority carrier lifetime is predicted to have an inverse relationship with doping concentration as found in Si [35]. As a result, the Ag doping may increase minority carrier lifetime and reduce the high recombination rate as it reduced the doping concentration from severely heavy doping level to a proper level [30, 35]. This was confirmed by TRPL measurement as shown in Figure 5. To analyse TRPL data, minority carrier lifetime τ decay formula is adopted [36, 37]:

$$\frac{dn}{dt} = -C_1 n - C_2 n^2, \tag{3}$$

where n is the minority carrier density, C_1, C_2 are the coefficients of linear and quadratic recombination process, and $C_1 = \tau^{-1}$.

The solution of (3) is the following equation [36, 37]:

$$n(t) = \frac{n_0 \exp(-t/\tau)}{1 + (C_2/C_1)\, n_0 \left[1 - \exp(-t/\tau)\right]}, \tag{4}$$

where n_0 is the initial excess carrier density. The initial sharp peak can be ascribed to Auger recombination due to very short duration of laser pulses and thus much high transient density. The time constant of the long tail section is the characteristic minority carrier lifetime of this material due to nonradiative decay via recombination centers at the surface, the back electrode interface, the grain boundaries, or deep defects within the grains. This characteristic minority carrier lifetime can be extracted through curve-fitting experimental data with (4). The lifetimes of samples with and without Ag are 8.98 ns and 6.42 ns, respectively, which is as expected. In short, Ag doping improved depletion region width and also minority carrier lifetime and therefore enhanced carrier collection efficiency significantly which benefits V_{OC}, J_{SC}, and efficiency.

Figure 6(a) demonstrates that V_{OC} is enhanced from 360 to 596 mV, J_{SC} from 11.63 to 14.36 mA/cm^2, FF from 33.8% to 41%, shunting resistance from 48 to 180 $\Omega{\cdot}cm^2$, and efficiency from 1.42% to 3.51% by incorporating this Ag layer. Low overall FF can be partly due to the unreacted Sn which induces shunting especially for porous structure. FF enhancement due to the Ag layer is mainly explained by the reduction of MoS_2. The Ag layer dragging down the doping level enlarges the depletion region and carrier diffusion length and therefore increases carrier collection efficiency, which improves both V_{OC} and J_{SC}. J_{SC} enhancement may be also accounted for by reduction of ZnS, SnS_{2-x} at the top surface region due to the Ag layer. Figure 6(b) reveals that the incorporation of Ag layer impairs the carrier collection for light of wavelength above 750 nm which is partly blamed by high refection in the same wavelength range. Moreover, the band gap of the absorber layer is determined from the intercept at the x-axis in the plot of $(E \times \mathrm{EQE})^2$ versus E where E is the photon energy and the result is illustrated in the inset table in Figures 6(a) and 6(c) [38]. The band gap of the sample with the Ag layer is 0.07 eV higher than that of the sample without the Ag layer, which implies the doping effect introduced by the Ag layer as $(Cu,Ag)_2ZnSnS_4$ should have a band gap higher than that of CZTS [39, 40]. This is another reason for V_{OC} enhancement. Besides this, $(Cu,Ag)_2ZnSnS_4$ has a band gap of ~1.6 eV as calculated, which means all absorption above 750 nm may be sub-band gap absorption and would contribute much less to free carrier generation. This may be the major reason that CZTS performs better than $(Cu,Ag)_2ZnSnS_4$ on EQE in wavelength range above 750 nm.

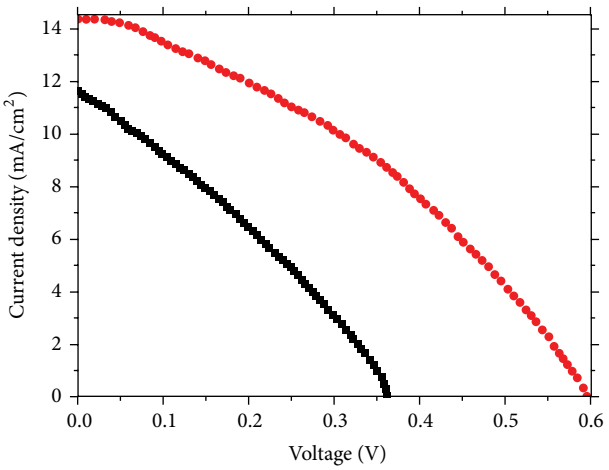

Structure	V_{OC} (mV)	J_{SC} (mA/cm^2)	EQE based J_{SC}	Shunt resistance R_{SH} (Ω·cm^2)	FF (%)	Efficiency η (%)	Band gap (eV)
Mo/CZTS	360	11.64	11.6	48	33.8	1.42	1.53
Mo/Ag/CZTS	596	14.38	14.36	180	41	3.51	1.6

(a)

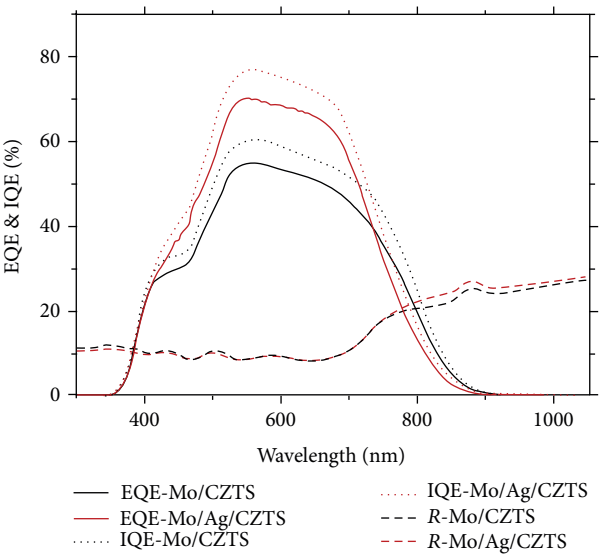

(b)

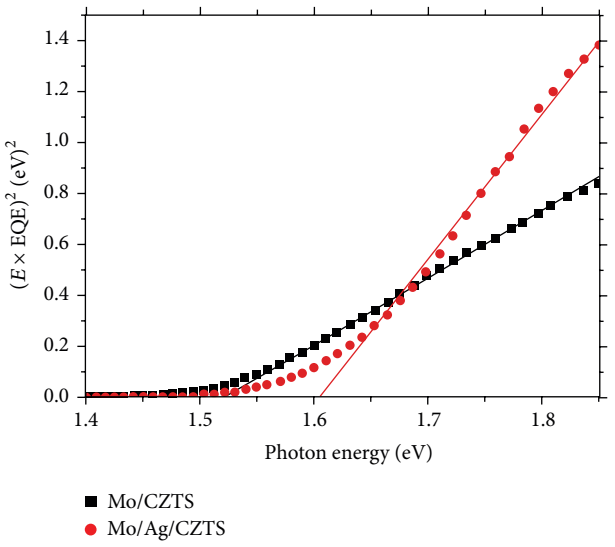

(c)

FIGURE 6: (a) Light J-V curve of the CZTS devices with and without the Ag intermediate layer measured at 25°C under AM 1.5 G illumination. The efficiency, V_{OC}, J_{SC}, FF, and shunt resistance R_{SH} are given in the inset table; (b) external quantum efficiency (EQE), internal quantum efficiency (IQE), and reflectance (R) of the CZTS solar cells with and without the Ag layer; and (c) band gap estimation plot $(E \times EQE)^2$ versus E, where E is the photon energy. Band gap results are also listed in the inset table in (a).

4. Conclusions

In summary, a 20 nm Ag intermediate layer between CZTS absorber and back contact was proved effective in enhancing evaporated CZTS solar cell performance dramatically. The Ag layer contributed to the reduction of MoS_2, ZnS, and SnS_{2-x}, which enhanced FF and carrier transport; simultaneously Ag also lowered doping of the absorber substantially as Ag introduced n-type doping compensating part of the p-type doping, which enlarged the depletion region, increased the lifetime of minority carrier, and therefore benefited both V_{OC} and J_{SC}. The V_{OC} improvement is partly due to the doping effect of the Ag layer because this layer also increased the band gap of the absorber from 1.53 eV to 1.6 eV. Consequently, it results in a significant efficiency increase from 1.42% to 3.51% though it degrades the crystallinity of the absorber

negligibly. The high shunting and low FF for both samples are mainly accounted for by unreacted Sn and porous structure of the absorber.

Disclosure

Responsibility for the views, information, or advice expressed herein is not accepted by the Australian Government.

Conflict of Interests

The authors declare that there is no conflict of interests regarding the publication of this paper.

Acknowledgments

This program has been supported by the Australian Government through the Australian Renewable Energy Agency (ARENA) and Australian Research Council (ARC) and Guodian New Energy Technology Research Institute, China Guodian Corporation. The authors acknowledge the facilities and the scientific and technical assistance of the Australian Microscopy & Microanalysis Research Facility at the Electron Microscope Unit, The University of New South Wales (UNSW). The authors acknowledge part of the metal precursor depositions by Mr. Kazuo Omaki of UNSW.

References

[1] L. M. Peter, "Towards sustainable photovoltaics: the search for new materials," *Philosophical Transactions of the Royal Society A*, vol. 369, p. 1840, 2011.

[2] J. P. Teixeira, R. A. Sousa, M. G. Sousa et al., "Radiative transitions in highly doped and compensated chalcopyrites and kesterites: the case of Cu_2ZnSnS_4," *Physical Review B*, vol. 90, Article ID 235202, 2014.

[3] J. J. Scragg, J. T. Wätjen, M. Edoff, T. Ericson, T. Kubart, and C. Platzer-Björkman, "A detrimental reaction at the molybdenum back contact in $Cu_2ZnSn(S,Se)_4$ thin-film solar cells," *Journal of the American Chemical Society*, vol. 134, no. 47, pp. 19330–19333, 2012.

[4] J. J. Scragg, T. Ericson, T. Kubart, M. Edoff, and C. Platzer-Björkman, "Chemical insights into the instability of Cu_2ZnSn_4 films during annealing," *Chemistry of Materials*, vol. 23, no. 20, pp. 4625–4633, 2011.

[5] J. T. Wätjen, J. J. Scragg, T. Ericson, M. Edoff, and C. Platzer-Björkman, "Secondary compound formation revealed by transmission electron microscopy at the Cu_2ZnSnS_4/Mo interface," *Thin Solid Films*, vol. 535, no. 1, pp. 31–34, 2013.

[6] J. J. Scragg, T. Kubart, J. T. Wätjen, T. Ericson, M. K. Linnarsson, and C. Platzer-Björkman, "Effects of back contact instability on Cu_2ZnSn_4 devices and processes," *Chemistry of Materials*, vol. 25, no. 15, pp. 3162–3171, 2013.

[7] C. Platzer-Björkman, J. Scragg, H. Flammersberger, T. Kubart, and M. Edoff, "Influence of precursor sulfur content on film formation and compositional changes in Cu_2ZnSnS_4 films and solar cells," *Solar Energy Materials and Solar Cells*, vol. 98, pp. 110–117, 2012.

[8] A. Walsh, S. Y. Chen, S. H. Wei, and X. G. Gong, "Kesterite thin-film solar cells: advances in materials modelling of Cu_2ZnSnS_4," *Advanced Energy Materials*, vol. 2, no. 4, pp. 400–409, 2012.

[9] D. B. Mitzi, O. Gunawan, T. K. Todorov, K. Wang, and S. Guha, "The path towards a high-performance solution-processed kesterite solar cell," *Solar Energy Materials and Solar Cells*, vol. 95, no. 6, pp. 1421–1436, 2011.

[10] B. Shin, N. A. Bojarczuk, and S. Guha, "On the kinetics of $MoSe_2$ interfacial layer formation in chalcogen-based thin film solar cells with a molybdenum back contact," *Applied Physics Letters*, vol. 102, no. 9, Article ID 091907, 2013.

[11] B. Shin, Y. Zhu, N. A. Bojarczuk, S. J. Chey, and S. Guha, "Control of an interfacial $MoSe_2$ layer in $Cu_2ZnSnSe_4$ thin film solar cells: 8.9% power conversion efficiency with a TiN diffusion barrier," *Applied Physics Letters*, vol. 101, no. 5, Article ID 053903, 2012.

[12] S. Lopez-Marino, M. Placidi, A. Perez-Tomas et al., "Inhibiting the absorber/Mo-back contact decomposition reaction in $Cu_2ZnSnSe_4$ solar cells: the role of a ZnO intermediate nanolayer," *Journal of Materials Chemistry A* , vol. 1, no. 29, pp. 8338–8343, 2013.

[13] W. Li, J. Chen, H. Cui, F. Liu, and X. Hao, "Inhibiting MoS_2 formation by introducing a ZnO intermediate layer for Cu_2ZnSnS_4 solar cells," *Materials Letters*, vol. 130, pp. 87–90, 2014.

[14] F. Liu, K. Sun, W. Li et al., "Enhancing the Cu_2ZnSnS_4 solar cell efficiency by back contact modification: inserting a thin TiB_2 intermediate layer at Cu_2ZnSnS_4/Mo interface," *Applied Physics Letters*, vol. 104, no. 5, Article ID 051105, 2014.

[15] H. Cui, X. Liu, F. Liu, X. Hao, N. Song, and C. Yan, "Boosting Cu_2ZnSnS_4 solar cells efficiency by a thin Ag intermediate layer between absorber and back contact," *Applied Physics Letters*, vol. 104, no. 4, Article ID 041115, 2014.

[16] W. Li, J. Chen, C. Yan, F. Liu, and X. Hao, "Transmission electron microscopy analysis for the process of crystallization of Cu_2ZnSn_4 film from sputtered Zn/CuSn precursor," *Nanotechnology*, vol. 25, no. 19, Article ID 195701, 2014.

[17] F. Liu, Y. Lai, J. Liu et al., "Characterization of chemical bath deposited CdS thin films at different deposition temperature," *Journal of Alloys & Compounds*, vol. 493, no. 1-2, pp. 305–308, 2010.

[18] K. L. Chopra, P. D. Paulson, and V. Dutta, "Thin-film solar cells: an overview," *Progress in Photovoltaics: Research and Applications*, vol. 12, no. 2-3, pp. 69–92, 2004.

[19] W. Li, X. Liu, H. Cui, S. Huang, and X. Hao, "The role of Ag in $(Ag,Cu)_2ZnSnS_4$ thin film for solar cell application," *Journal of Alloys and Compounds*, vol. 625, pp. 277–283, 2015.

[20] Z. Johan and P. Picot, "Pirquitasite, Ag_2ZnSnS_4 a new member of the stannite group," *Bulletin de Minéralogie*, vol. 105, p. 229, 1982.

[21] H. Cui, W. Li, X. Liu et al., "Optimization of precursor deposition for evaporated Cu_2ZnSnS_4 solar cells," *Applied Physics A*, 2014.

[22] A. Fairbrother, X. Fontané, V. Izquierdo-Roca et al., "On the formation mechanisms of Zn-rich Cu2ZnSnS4 films prepared by sulfurization of metallic stacks," *Solar Energy Materials and Solar Cells*, vol. 112, pp. 97–105, 2013.

[23] T. P. Dhakal, C.-Y. Peng, R. Reid Tobias, R. Dasharathy, and C. R. Westgate, "Characterization of a CZTS thin film solar cell grown by sputtering method," *Solar Energy*, vol. 100, pp. 23–30, 2014.

[24] J. J. Scragg, P. J. Dale, L. M. Peter, G. Zoppi, and I. Forbes, "New routes to sustainable photovoltaics: evaluation of Cu_2ZnSnS_4 as

an alternative absorber material," *Physica Status Solidi B: Basic Research*, vol. 245, no. 9, pp. 1772–1778, 2008.

[25] P. A. Fernandes, P. M. P. Salomé, A. F. da Cunha, and B.-A. Schubert, "Cu_2ZnSnS_4 solar cells prepared with sulphurized dc-sputtered stacked metallic precursors," *Thin Solid Films*, vol. 519, no. 21, pp. 7382–7385, 2011.

[26] T. Kobayashi, K. Jimbo, K. Tsuchida, S. Shinoda, T. Oyanaoi, and H. Katagiri, "Investigation of Cu_2ZnSnS_4-based thin film solar cells using abundant materials," *Japanese Journal of Applied Physics*, vol. 44, no. 1, pp. 783–787, 2005.

[27] T. Tanaka, T. Nagatomo, D. Kawasaki et al., "Preparation of Cu_2ZnSnS_4 thin films by hybrid sputtering," *Journal of Physics and Chemistry of Solids*, vol. 66, no. 11, pp. 1978–1981, 2005.

[28] J. Vidal, S. Lany, M. D'Avezac et al., "Band-structure, optical properties, and defect physics of the photovoltaic semiconductor SnS," *Applied Physics Letters*, vol. 100, no. 3, Article ID 032104, 2012.

[29] K. T. Ramakrishna Reddy, N. Koteswara Reddy, and R. W. Miles, "Photovoltaic properties of SnS based solar cells," *Solar Energy Materials and Solar Cells*, vol. 90, no. 18-19, pp. 3041–3046, 2006.

[30] O. Gunawan, T. Gokmen, and D. B. Mitzi, "Suns-V_{OC} characteristics of high performance kesterite solar cells," *Journal of Applied Physics*, vol. 116, no. 8, Article ID 084504, 2014.

[31] L.-Y. Yeh and K.-W. Cheng, "Preparation of the Ag-Zn-Sn-S quaternary photoelectrodes using chemical bath deposition for photoelectrochemical applications," *Thin Solid Films*, vol. 558, pp. 289–293, 2014.

[32] T. Sasamura, T. Osaki, T. Kameyama et al., "Solution-phase synthesis of stannite-type Ag_2ZnSnS_4 nanoparticles for application to photoelectrode materials," *Chemistry Letters*, vol. 41, no. 9, pp. 1009–1011, 2012.

[33] S. Ikeda, T. Nakamura, T. Harada, and M. Matsumura, "Multi-component sulfides as narrow gap hydrogen evolution photocatalysts," *Physical Chemistry Chemical Physics*, vol. 12, no. 42, pp. 13943–13949, 2010.

[34] B. Shin, O. Gunawan, Y. Zhu, N. A. Bojarczuk, S. J. Chey, and S. Guha, "Thin film solar cell with 8.4% power conversion efficiency using an earth-abundant Cu_2ZnSnS_4 absorber," *Progress in Photovoltaics: Research and Applications*, vol. 21, no. 1, pp. 72–76, 2013.

[35] J. Wong, J. L. Huang, B. Eggleston et al., "Lifetime limiting recombination pathway in thin-film polycrystalline silicon on glass solar cells," *Journal of Applied Physics*, vol. 107, no. 12, Article ID 123705, 2010.

[36] O. Gunawan, T. K. Todorov, and D. B. Mitzi, "Loss mechanisms in hydrazine-processed $Cu_2ZnSn(Se,S)_4$ solar cells," *Applied Physics Letters*, vol. 97, no. 23, Article ID 233506, 2010.

[37] B. Ohnesorge, R. Weigand, G. Bacher, A. Forchel, W. Riedl, and F. H. Karg, "Minority-carrier lifetime and efficiency of $Cu(In,Ga)Se_2$ solar cells," *Applied Physics Letters*, vol. 73, no. 9, pp. 1224–1226, 1998.

[38] S. Ahmed, K. B. Reuter, O. Gunawan, L. Guo, L. T. Romankiw, and H. Deligianni, "A high efficiency electrodeposited Cu_2ZnSnS_4 solar cell," *Advanced Energy Materials*, vol. 2, no. 2, pp. 253–259, 2012.

[39] I. Tsuji, Y. Shimodaira, H. Kato, H. Kobayashi, and A. Kudo, "Novel stannite-type complex sulfide photocatalysts A^I_2-Zn-A^{IV}-S4 (A^I = Cu and Ag; A^{IV} = Sn and Ge) for hydrogen evolution under visible-light irradiation," *Chemistry of Materials*, vol. 22, no. 4, pp. 1402–1409, 2010.

[40] K. Li, B. Chai, T. Peng, J. Mao, and L. Zan, "Synthesis of multi-component sulfide Ag_2ZnSnS_4 as an efficient photocatalyst for H_2 production under visible light irradiation," *RSC Advances*, vol. 3, no. 1, pp. 253–258, 2013.